



HAL
open science

Structure of a Flat Plate Boundary Layer Subjected to Free-Stream Turbulence

Frédéric Péneau, Henri Claude Boisson, Alain Kondjoyan, Ned Djilali

► **To cite this version:**

Frédéric Péneau, Henri Claude Boisson, Alain Kondjoyan, Ned Djilali. Structure of a Flat Plate Boundary Layer Subjected to Free-Stream Turbulence. *International Journal of Computational Fluid Dynamics*, 2007, 18 (2), pp.175-188. 10.1080/10618560310001634177 . hal-02952882

HAL Id: hal-02952882

<https://hal.inrae.fr/hal-02952882>

Submitted on 17 May 2021

HAL is a multi-disciplinary open access archive for the deposit and dissemination of scientific research documents, whether they are published or not. The documents may come from teaching and research institutions in France or abroad, or from public or private research centers.

L'archive ouverte pluridisciplinaire **HAL**, est destinée au dépôt et à la diffusion de documents scientifiques de niveau recherche, publiés ou non, émanant des établissements d'enseignement et de recherche français ou étrangers, des laboratoires publics ou privés.



Distributed under a Creative Commons Attribution 4.0 International License

Structure of a Flat Plate Boundary Layer Subjected to Free-Stream Turbulence

FRÉDÉRIC PÉNEAU^{a,*}, HENRI CLAUDE BOISSON^b, ALAIN KONDOYAN^c and NED DJILALI^d

^aCERAM EAI Tech, 157 rue Albert Einstein, BP 085, 06902 Sophia Antipolis Cedex, France; ^bIMFT, av Pr Camille Soula, 31400 Toulouse, France; ^cINRA, S.R.V., 63122 Saint Genès Champanelle, France; ^dDepartment of Mechanical Engineering, University of Victoria, Victoria, BC, Canada V8W 3P6

The structure near the flat plate leading edge of an incompressible boundary layer subjected to free-stream turbulence is investigated using large eddy simulation (LES) with a dynamic mixed subgrid-scale model. Free-stream turbulent intensities ranging from 1.5 to 10% are investigated. The evolutions of the velocity, temperature and turbulent intensity profiles inside the boundary layer and the characteristic length scales are analyzed and compared to a laminar flat plate boundary layer. The impact of the free-stream turbulence is examined for Reynolds numbers ranging from 0 (leading edge of the flat plate) to $Re_x = 80,000$ by using two consecutive spatial LESs. Bypass transition is found to occur in the early stage of the boundary layer development for all five cases presented here. The analysis indicates that the thermal turbulent structures transfer more energy and hence generate more thermal fluctuations in their wake than the dynamic structures.

Keywords: Heat transfer; Free-stream turbulence; Flat plate boundary layer; Large eddy simulations

NOMENCLATURE

| | | | |
|---|---|---|---|
| C_f | Friction coefficient with free-stream turbulence | $Re_\theta = \frac{U_e \theta}{\nu}$ | Reynolds number based on the local momentum thickness θ |
| C_{f0} | Friction coefficient without free-stream turbulence | St | Stanton number with free-stream turbulence |
| $D = \frac{\lambda}{\rho C_p}$ | Thermal diffusivity | St_0 | Stanton number without free-stream turbulence |
| D_t | Subgrid diffusivity, turbulent diffusivity = $\langle v'T' \rangle / \partial T / \partial y$ | $T = T_{\text{mean}} + T'$ | Reynolds decomposition for the temperature field |
| $Iu = \frac{\sqrt{u_{\text{rms}}^2 + v_{\text{rms}}^2 + w_{\text{rms}}^2}}{U_e}$ | Turbulent intensity | T_{mean} | Mean temperature |
| h, h_e, h_w | Fluid enthalpy, free-stream fluid enthalpy and wall fluid enthalpy | T' | Temperature fluctuations $\langle T' \rangle = 0$ |
| $L_\varepsilon = \frac{\langle q_e^2 \rangle^{3/2}}{U_e \frac{\partial \langle q_e^2 \rangle}{\partial x}}$ | Free-stream turbulence dissipative length-scale | $T_{\text{rms}} = \langle T'T' \rangle^{0.5}$ | Temperature turbulent level |
| $P = \bar{P} + P''$ | Large eddy decomposition for the pressure field | $T = \bar{T} + T''$ | Large eddy decomposition for the temperature field |
| \bar{P} | Resolved pressure field | \bar{T} | Resolved temperature field |
| P'' | Subgrid pressure field | T'' | Subgrid temperature field |
| $Pr = \frac{\nu}{D}$ | Prandtl number | $Tu = \frac{u_{\text{rms}}}{U_e}$ | Turbulent level |
| $Pr_t = \frac{\nu_t}{D_t}$ | Turbulent Prandtl number | $u_i = U_i + u'_i$ | Reynolds decomposition for the velocity field |
| $q_e = \frac{u_{\text{rms}}^2 + v_{\text{rms}}^2 + w_{\text{rms}}^2}{2}$ | Turbulent kinetic energy | U_i | Mean velocity field; $U_1 = U$ longitudinal direction; $U_2 = V$ lateral direction; $U_3 = W$ span-wise direction |
| $Re_x = \frac{U_e x}{\nu}$ | Reynolds number based on the distance from the leading edge 'x' | | |

*Corresponding author. E-mail: frederic.peneau@cote-azur.cci.fr

| | | | |
|---|--|--|---|
| u'_i Velocity fluctuations $\langle u'_i \rangle = 0$ U_e | $u'_1 = u'$ longitudinal direction; $u'_2 = v'$ lateral direction; $u'_3 = w'$ spanwise direction. Mean free-stream longitudinal velocity component | $\delta_3 = \int_0^\infty \frac{U}{U_e} \times \left(1 - \left(\frac{U}{U_e}\right)^2\right) dy$ | Kinetic energy thickness |
| $u_i = \bar{u}_i + u''_i$ | Large eddy decomposition for the velocity field | $\Delta = \int_0^\infty \frac{U}{U_e} \left(\frac{h_e - h}{h_e - h_w}\right) dy$ | Enthalpy thickness |
| \bar{u}_i | Resolved velocity field | $\theta = \int_0^\infty \frac{U}{U_e} \left(1 - \frac{U}{U_e}\right) dy$ | Momentum thickness |
| u''_i | Subgrid velocity field | λ | Thermal conductivity |
| $u_{\text{rms}} = \langle u'_1 u'_1 \rangle^{0.5}$ | Longitudinal turbulent fluctuations | μ | Dynamic viscosity |
| $v_{\text{rms}} = \langle u'_2 u'_2 \rangle^{0.5}$ | Lateral turbulent fluctuations | $\nu = \frac{\mu}{\rho}$ | Kinematic viscosity |
| $w_{\text{rms}} = \langle u'_3 u'_3 \rangle^{0.5}$ | Span-wise turbulent fluctuations | ν_t | Subgrid viscosity, turbulent viscosity = $\langle u'v' \rangle / \partial U / \partial y$ |
| δ | Dynamic boundary layer thickness | ρ | Fluid density |
| δ_T | Thermal boundary layer thickness | $\langle \rangle$ | Average operator in the span-wise direction and in time |
| $\delta_1 = \int_0^\infty \left(1 - \frac{U}{U_e}\right) dy$ | Displacement thickness | | |

INTRODUCTION

The influence of high free-stream turbulence on the dynamics and heat transfer of boundary layer flows is relevant to many industrial applications and has been the subject of experimental and theoretical research for some time. The first studies were performed in the thirties by Fage and Falkner (1931) who did not observe any influence on heat transfer in the presumed laminar region. Due to discrepancies and contradictions in reported findings, the field remained wide open until the landmark work of Bradshaw (1974). In a series of studies with his team, (Simonich and Bradshaw, 1978; Hancock and Bradshaw, 1983, 1989; Baskaran *et al.*, 1989), Bradshaw and his group analyzed the influence of free-stream turbulence not only in terms of the turbulence level Tu but also in terms of the turbulent length scale L_e . It was found that if L_e is too small with respect to the boundary layer length scale, then the free-stream turbulent structures dissipate before reaching the surface of the plate with no increase in the dynamic activities of the flow or in heat transfer. In his report of 1974, Bradshaw noted the importance of the work of Charnay *et al.* (1971, 1972, 1976) on the interaction mechanisms between the free-stream flow and the wake of the boundary layer. A few years later, Dyban *et al.* (1977), Dyban and Epick (1985) published a very interesting and original work on the influence of free-stream turbulence on the laminar region of the boundary layer. With the focus of both academic and industrial research at that time on turbulent flow, Dyban *et al.*'s work did not receive the attention it deserved. An increase of 56% in the friction coefficient was observed at low Reynolds numbers ($< 20,000$) with a free-stream turbulence level of 12.5%. These results underscored the importance of the interaction between the boundary layer and the free-stream near the leading edge. Meanwhile, a consensus has emerged from the numerous studies on

turbulent boundary layers. Free-stream turbulence does increase the dynamic and heat transfer in the turbulent boundary layer and heat transfer seems to be more sensitive to free-stream turbulence (Pédissius *et al.*, 1979; Meier and Kreplin, 1980; Blair, 1983a,b). Although this conclusion is general, there is considerable variation from study to study on the magnitude of the heat transfer enhancement. Several studies in the 80s and 90s attempted to model these phenomena with varying success (Young *et al.*, 1992; Maciejewski and Moffat, 1992). A review of the main experimental work can be found in Kondjoyan *et al.* (2002).

In this paper we present a numerical analysis of the influence of free-stream turbulence on the "laminar" boundary layer. Our results are compared to the experimental data of Dyban *et al.* (1977) and Dyban and Epick (1985) and we propose an interpretation of the observed phenomena. The paper provides first an overview of the numerical model, the computational procedure and the physical characteristics of the problem. We then present the evolution of the velocity and temperature profiles inside the boundary layer in the presence of free-stream turbulence. The turbulent intensity and turbulent energy production profiles are examined and compared to those for a turbulent boundary layer with no free-stream turbulence. Finally, a physical interpretation of the results is proposed based on an analysis of the Reynolds stresses and turbulent Prandtl number.

NUMERICAL METHOD AND SUBGRID MODELING

The LES Equations and the Subgrid-scale Model

The LES equations are obtained by introducing the following decomposition in the Navier–Stokes equations:

$$u_i = \bar{u}_i + u''_i \quad (1)$$

where \bar{u}_i represents the implicitly filtered, resolved velocity field, and u_i' represents the subgrid velocity field. This yields:

$$\frac{\partial \bar{u}_i}{\partial x_i} = 0 \quad (2)$$

$$\frac{\partial \bar{u}_i}{\partial t} + \frac{\partial \bar{u}_i \bar{u}_j}{\partial x_j} = -\frac{\partial \bar{p}}{\partial x_i} + \frac{\partial (2\nu \bar{S}_{ij} - \tau_{ij})}{\partial x_j} \quad (3)$$

where

$$\tau = \overline{u_i u_j} - \bar{u}_i \bar{u}_j = L_{ij} + C_{ij} + R_{ij} \quad (4)$$

with

$$L_{ij} = \overline{\bar{u}_i \bar{u}_j} - \bar{u}_i \bar{u}_j \quad (5)$$

$$C_{ij} = \overline{\bar{u}_i u_j'} + \overline{\bar{u}_j u_i'} - \left(\overline{\bar{u}_i u_j'} + \overline{\bar{u}_j u_i'} \right) \quad (6)$$

$$R_{ij} = \overline{u_i' u_j'} - \bar{u}_i' \bar{u}_j' \quad (7)$$

$$\bar{p} = \bar{P} + (C_{kk} + R_{kk})/3. \quad (8)$$

L_{ij} is calculated explicitly, while C_{ij} and R_{ij} are modeled using the classical concept of subgrid viscosity ν_t proposed by Smagorinsky (1963) in conjunction with the dynamic mixed model (DMM) of Zang *et al.* (1993):

$$C_{ij} + R_{ij} = -\nu_t \bar{S}_{ij} \quad \text{for } i \neq j. \quad (9)$$

With this model ν_t is a function of space and time. C_{kk} and R_{kk} are incorporated into the pressure terms because of the incompressibility condition. For further details on the DMM and the calculation procedure for evaluating ν_t , the reader is referred to Péneau *et al.* (1999). The introduction of a similar decomposition into the energy equation yields:

$$\frac{\partial \bar{T}}{\partial t} + \frac{\partial \bar{T} \bar{u}_j}{\partial x_j} = \frac{\partial \left(D \frac{\partial \bar{T}}{\partial x_j} \right) - q_j}{\partial x_j} \quad (10)$$

with

$$q_j = \overline{\bar{T} u_j} = \bar{T} \bar{u}_j = Lc_j + Cc_j + Rc_j. \quad (11)$$

Again, Lc_j is calculated explicitly while Cc_j and Rc_j are modeled using

$$Cc_j + Rc_j = -D_t \frac{\partial \bar{T}}{\partial x_j}. \quad (12)$$

The Numerical Method

The numerical simulations are carried out using JADIM code (Calmet and Magnaudet, 1996). The momentum and scalar equations are discretized using a finite volume method with a second-order centered scheme on a staggered grid. The solution is advanced in time using a three-step Runge-Kutta procedure. The nonlinear terms are

computed explicitly while the diffusive terms are calculated using the semi-implicit Crank-Nicholson algorithm. To satisfy the incompressibility condition, a Poisson equation is solved by combining a direct inversion in the (x,y) (longitudinal and lateral direction, respectively) plane with a spectral Fourier method in the third direction z (transversal direction). For more details on JADIM the reader is referred to Calmet and Magnaudet (1996).

Grid and Physical Parameter

The grid on which the spatial simulations are performed was initially designed to simulate a fully turbulent boundary layer with entrance Reynolds number, based on the displacement thickness δ_1 , $Re_{\delta_1} = 1620$. The dimensions of this domain are $L_x = 85\delta_1$, $L_y = 50\delta_1$ and $L_z = 20\delta_1$ with the following number of mesh points in the three direction $N_x = 96$, $N_y = 96$ and $N_z = 64$. In wall units, the mesh size in the longitudinal and span-wise directions is $\Delta x^+ = (\Delta x \cdot u_\tau) / (\nu) = 38$ and $\Delta z^+ = 24$. In the previous equation u_τ is the friction velocity of a fully turbulent boundary layer at $Re_{\delta_1} = 1620$. Near the wall, the mesh is refined in the normal direction, with the first point located at $y^+ = 0.18$. The physical dimensions are $L_x = 1.7$ m, $L_y = 1$ m, $L_z = 0.4$ m and $\Delta x = 1.04 \times 10^{-2}$ m and $\Delta z = 0.625 \times 10^{-2}$ m. This mesh, which proved to be well adapted for the simulation of a fully turbulent boundary layer (Péneau *et al.*, 1999), is used to simulate the development under an air flow ($Pr = 0.72$) boundary layer near the leading edge of a flat plate subjected to a free-stream turbulent field. The mean free-stream velocity is $U_e = 1.23$ m/s. The free-stream temperature is $T_e = 273$ K while the wall temperature is set to $T_w = 274$ K. Open boundary conditions are set as $\partial^2 \bar{u}_i / \partial n^2 = 0$, where n is the direction normal to the exit plane.

THE HIGH FREE-STREAM TURBULENCE FIELD AND THE SPATIAL SIMULATION OF THE BOUNDARY LAYER

The generation of the turbulent fields used as entrance conditions for our spatial large eddy simulation (LES) has been fully presented in Péneau *et al.* (2000). The same method was used here, utilizing the computational mesh described in the preceding section so that a larger range of length scale is covered and a better resolution of the vortices is achieved in the region near the wall. The resulting free-stream turbulence field as well as the boundary conditions used for the simulation are shown in Fig. 1. The velocity field corresponding to the middle yz plane is recorded for 1000 time steps, and is then used as an entrance condition for the spatial simulation of the boundary layer development.

Five cases of free-stream turbulence have been generated this way. Table I presents their turbulent characteristics.

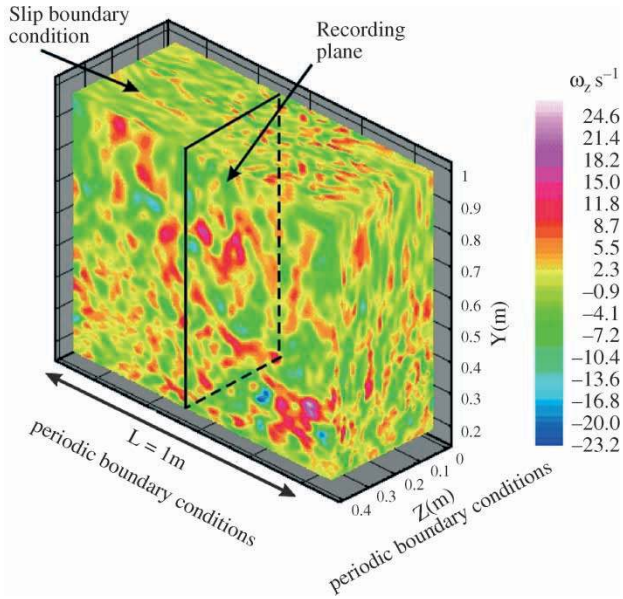


FIGURE 1 Lateral component of a typical free-stream vorticity field. (Colour version available to view online.)

Figures 2 and 3 show the turbulence level and intensity profiles for the five cases of free-stream turbulent fields investigated, and Fig. 4 shows the temporal evolution. The profiles presented were obtained by applying an averaging operator in the span-wise direction and in time (1000 time steps). “ $y = 0\text{ m}$ ” corresponds to the position of the flat plate while “ $y = 1\text{ m}$ ” corresponds to the north boundary of the domain of calculation. In this direction, the mesh size increases progressively and hence there is a decrease in the turbulent levels and intensities as we reach the north boundary.

This phenomenon is less important for cases D and E because these turbulent fields were generated with larger vortices which are better resolved and do not dissipate as much in this region. The root mean square velocity profiles for the five cases indicate that the turbulent fields are almost isotropic and homogeneous except near the north and south boundaries of the domain, again because of the boundary conditions imposed there. Note that a constant free-stream temperature field is imposed such that no *rms* temperature profile exists.

TABLE I Turbulent characteristics of the five free-stream turbulent fields generated

| | Tu in % | Iu in % |
|---------|-----------|-----------|
| Case A | 1 | 2 |
| Case B | 3 | 5 |
| Case C* | 3 | 5 |
| Case D | 5 | 8 |
| Case E | 10 | 16 |

*The case C was generated with bigger vortices to analyse the influence of the turbulence length-scale on the wall transfer.

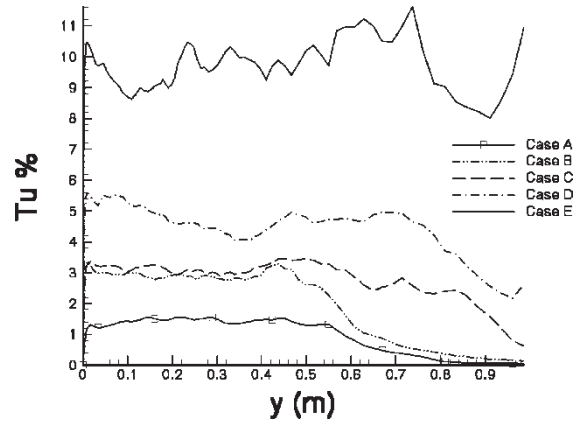


FIGURE 2 Turbulent level profiles.

The temporal evolution obtained by applying an averaging operator in the span-wise and lateral direction on the entrance velocity signals shows an exponential decay of the turbulence level similar to the spatial decay of grid-generated turbulence.

In order to extend the Reynolds number of the simulations, two successive spatial simulations were

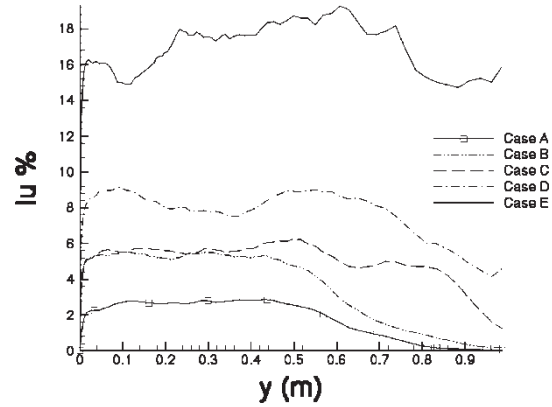


FIGURE 3 Turbulent intensity profiles.

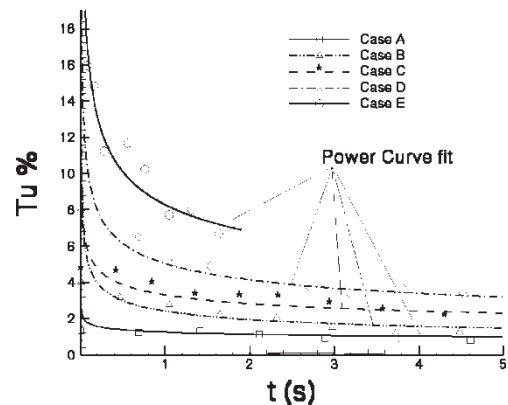


FIGURE 4 Temporal evolution of the turbulence levels.

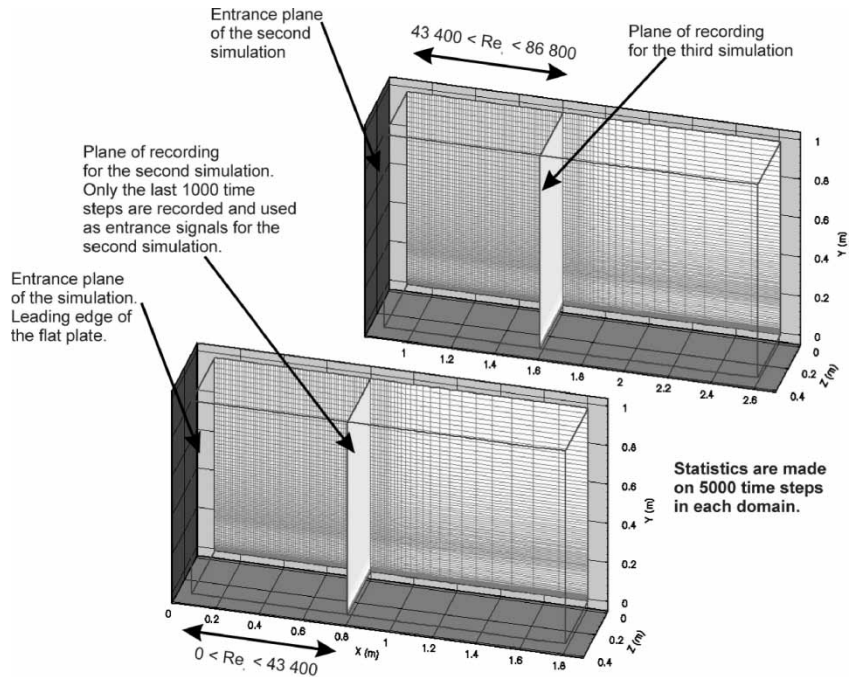


FIGURE 5 Method for spatial large eddy simulation by consecutive calculations.

performed as shown in Fig. 5. In the first domain of calculation (the bottom domain in Fig. 5) the 1000 time steps recorded from the free-stream turbulence field generation are used as entrance signal at the west boundary of the domain. At the south boundary, a no slip condition is imposed so that the arrival of a free-stream turbulence field on the leading edge of a flat plate is simulated. However, in order to avoid numerical instabilities, the no slip boundary condition on the longitudinal velocity component as well as the constant temperature condition are imposed progressively on the first cells of the domain in the x direction. The resulting gradual “transition” can be observed in Figs. 6 and 7. Spatial LESs of a laminar boundary layer with no free-stream turbulence have been performed on the same domains with the same subgrid-scale model for $0 \leq Re_x \leq 200,000$ and have yielded perfect agreement with Blasius’ solution.[†] Those simulations were performed using five successive simulations. The first two are used as initial fields for the simulations presented in the next paragraph.

The LESs were performed in the following way. For each domain only half of the box is considered as the last 16 cells in the longitudinal direction are progressively stretched before reaching the outflow boundary condition as one can observe in Fig. 5. For the calculation in the first domain ($0 \leq Re_x \leq 43,400$), we start with the laminar boundary layer solution. The calculation is initiated and the free-stream turbulent field enters the domain. The interaction of the free-stream turbulence with the laminar boundary layer then takes place. After 2000 time steps (requiring input from two calculations of 1000 time steps to impose

recorded entrance signals) we start to compute the statistics over 5000 time steps. During the last 1000 time steps, velocity and temperature signals are also recorded to be used as entrance signals for the second calculation domain ($43,400 \leq Re_x \leq 86,800$). With this method, if the statistics at the exit of the first domain of calculation are not equivalent to those at the entrance of the second one, this implies that the flow was not statistically converged in the first domain. For the second simulation we proceed in the same manner except that now the initial field is the one obtained without free-stream turbulence for $43,400 \leq Re_x \leq 86,800$.

RESULTS

Figures 6 and 7 show instantaneous velocity and temperature fields for case E ($Tu \approx 10\%$) for Reynolds number varying from 0 ($x = 0$ m) up to 50,000 ($x \approx 0.9$ m). As observed earlier, the free-stream flow is maintained at a constant temperature. The formation of streak-like structures takes place rapidly after the leading edge for both fields. This supports the occurrence of bypass transition pointed out in Péneau *et al.* (2000).

In Figs. 8 and 9, ejection phenomena of equal intensity for both fields are observed.

Selective results representative of the evolution of the flow with the turbulence level are presented next. Figure 10 shows that up to $Re_x = 73,000$ the mean longitudinal velocity profiles remain virtually insensitive to low turbulence level. With increasing turbulent level

[†]If we disregard the statistics in the first cell of the domain where the no slip condition is progressively imposed.

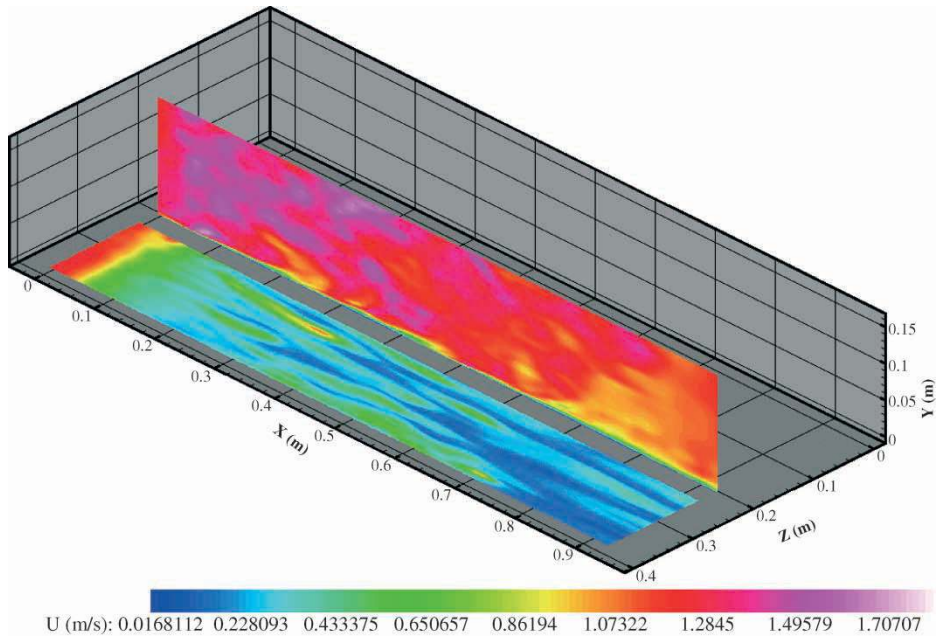


FIGURE 6 Instantaneous xy and zx plane velocity field; case E.

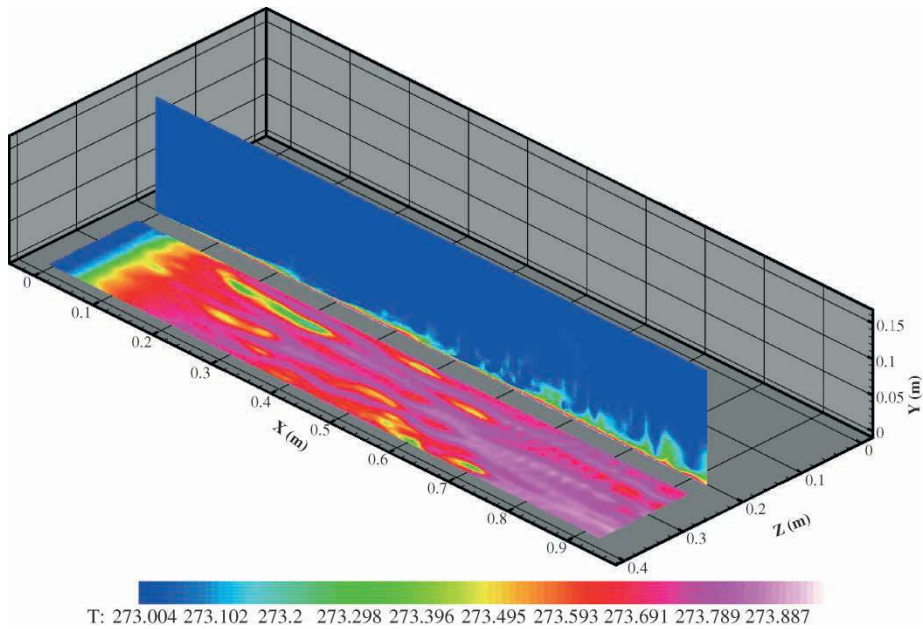


FIGURE 7 Instantaneous xy and zx plane temperature field; case E.

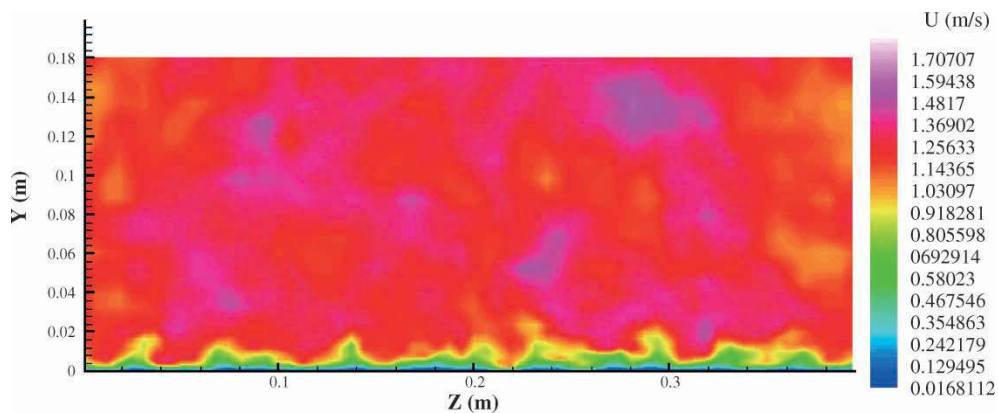


FIGURE 8 Instantaneous zy plane x velocity field at $Re_x \approx 40,000$; case E. (Colour version available to view online.)

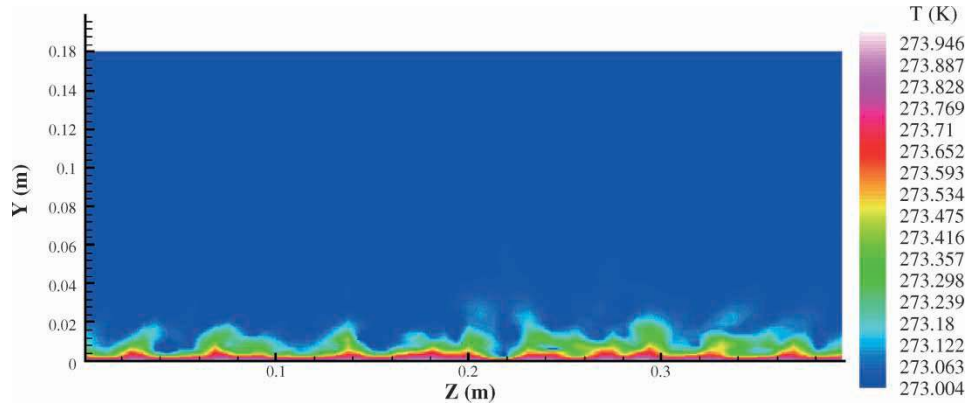


FIGURE 9 Instantaneous zy plane temperature field at $Re_x \approx 40,000$; case E. (Colour version available to view online.)

(shown in Fig. 11), a progressive flattening of the velocity profile takes place inducing the formation of a wake. The wake formation was also observed experimentally by Dyban *et al.* (1977) and Dyban and Epick (1985) shown in Fig. 12.

Figure 13 shows a more pronounced flattening of the temperature profile compared to the velocity profile. This was reported in Péneau *et al.* (2000) and is confirmed here with the finer grid simulations presented for both lower turbulent levels and higher Reynolds numbers. At higher turbulence levels we can observe in Fig. 14 that for case E, the profile is closer to a turbulent profile even though no logarithmic region is yet apparent.

The spatial evolution of the boundary layer thicknesses is plotted in Figs. 15 and 16. The absence of discontinuities around $Re_x \approx 40,000$ proves, at least up to $Re_x = 80,000$, that the consecutive simulations methodology used does not perturb the spatial evolution. It also shows that at a moderate turbulent level, there is no significant thickening of the boundary layer in contrast with higher turbulence levels. The thickening explains the flattening of the velocity profile and, consequently, the reduction of the displacement thickness and increase of momentum thickness. The corresponding phenomena for

the thermal field are even more important, hence the higher flattening of the temperature profile (Fig. 17) when the boundary layer thickness is used for normalizing the data.

The higher thickening of the thermal boundary layer is explained by the value of the turbulent Prandtl number inside the boundary layer. As shown in Figs. 18 and 19, whereas Pr_t is close to 1 at low turbulence levels, $Pr_t < 1$ over most of the boundary layer at a higher turbulence level, such as in case E. This implies the thermal turbulent structures transfer more energy and hence generate higher fluctuations in their wake than the dynamic structures.

Although at low turbulence levels no thickening of the boundary layer and no flattening of the velocity profile is observed, there are nevertheless some important phenomena that occur inside the boundary layer. Figures 20–22 show that a rapid increase of the maximum turbulence level takes place inside the boundary layer, and values exceeding free-stream levels are attained. This points to a mechanism of turbulent energy production inside the boundary layer. These observations are consistent with the experimental measurements of Dyban *et al.* (1977) (see Fig. 23).

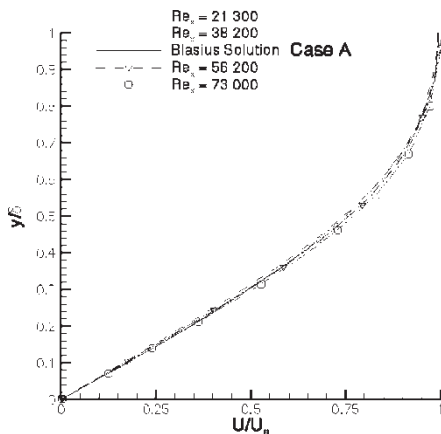


FIGURE 10 U velocity profile spatial evolution for case A.

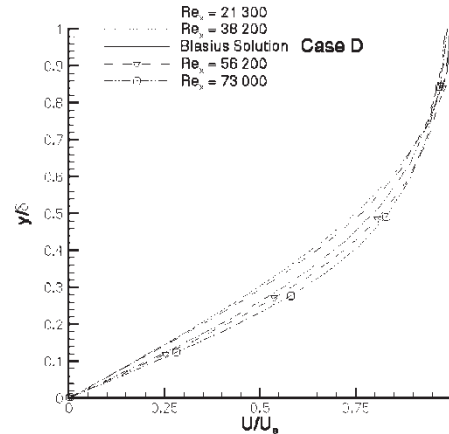


FIGURE 11 U velocity profile spatial evolution for case D.

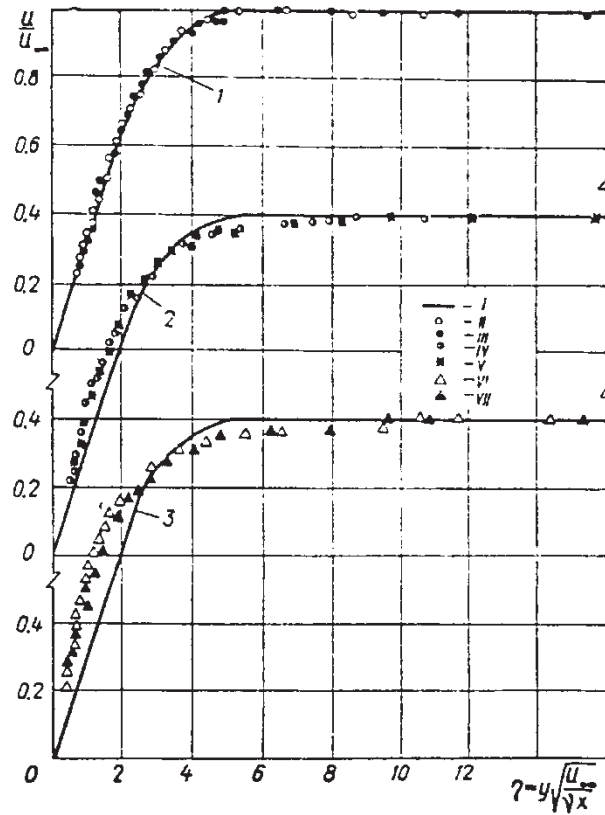


Fig. 1. Distribution of the velocities in the laminar boundary layer: I—Blasius profile; II— $Re_\infty = 19,900, \sqrt{(u'_\infty)^2}/U_\infty = 0.3\%$; III— $Re_\infty = 6,150, \sqrt{(u'_\infty)^2}/U_\infty = 0.31\%$; IV— $Re_\infty = 19,950, \sqrt{(u'_\infty)^2}/U_\infty = 3.66\%$; V— $Re_\infty = 6,160, \sqrt{(u'_\infty)^2}/U_\infty = 4.41\%$; VI— $Re_\infty = 19,900, \sqrt{(u'_\infty)^2}/U_\infty = 12.47\%$; VII— $Re_\infty = 6,300, \sqrt{(u'_\infty)^2}/U_\infty = 9.69\%$.

FIGURE 12 Extracted from Dyban *et al.* (1977) (legend from the article has been kept).

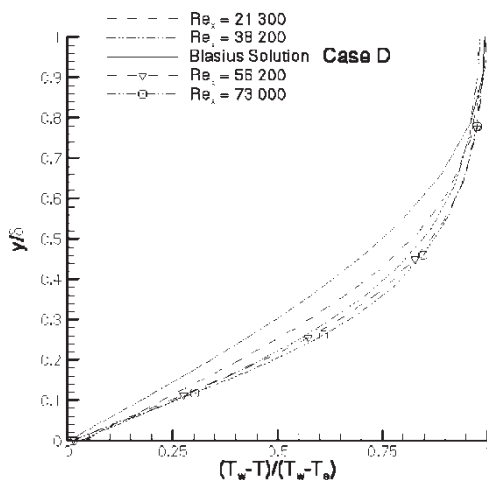


FIGURE 13 Temperature profile spatial evolution for case D.

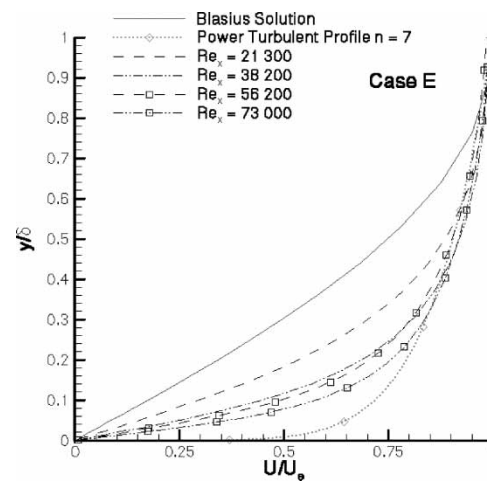


FIGURE 14 U velocity profile spatial evolution for case E.

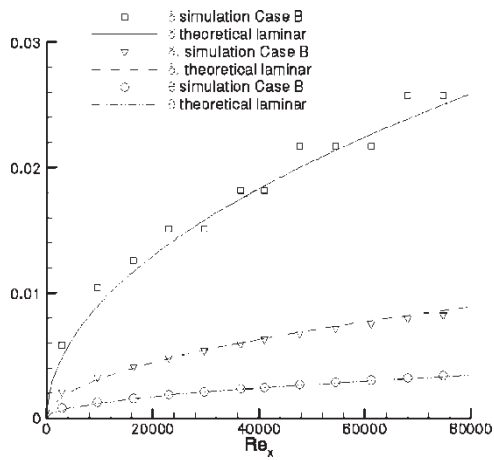


FIGURE 15 Spatial evolution of the boundary layer thicknesses (in m) for case B.

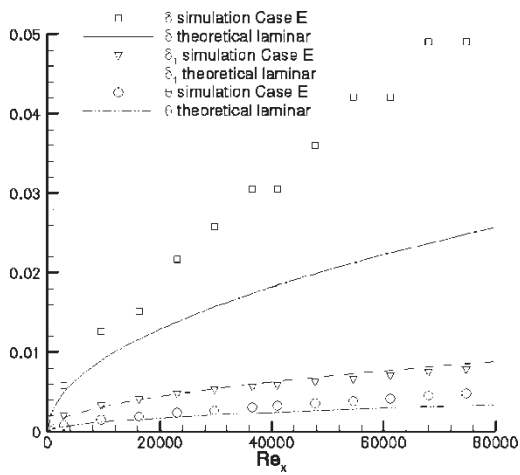


FIGURE 16 Spatial evolution of the boundary layer thicknesses (in m) for case E.

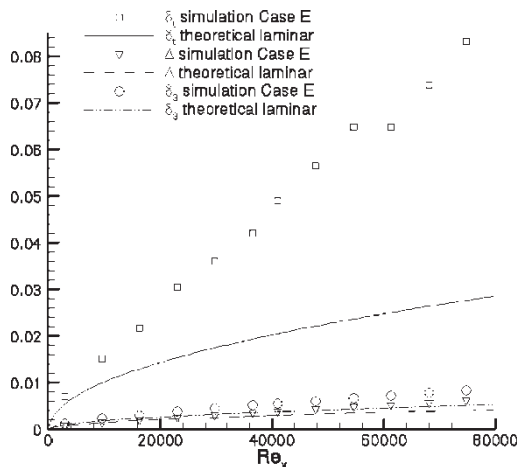


FIGURE 17 Spatial evolution of the thermal boundary layer thicknesses (in m) for case E.

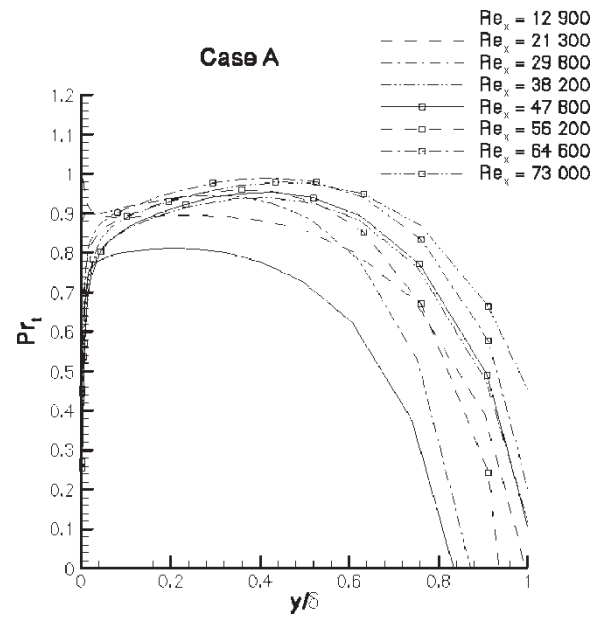


FIGURE 18 Spatial evolution of the turbulent Prandtl number for case A.

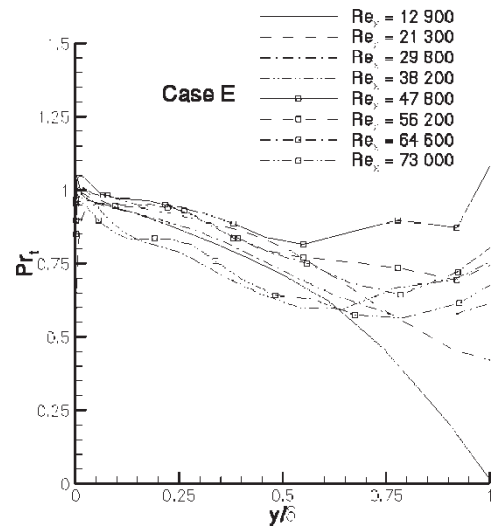


FIGURE 19 Spatial evolution of the turbulent Prandtl number for case E.

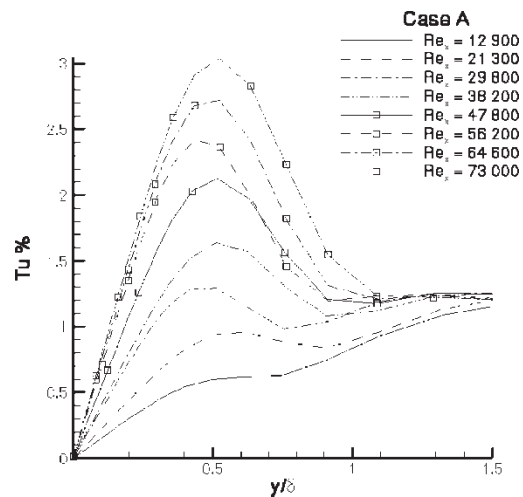


FIGURE 20 Spatial evolution of the turbulent level for case A.

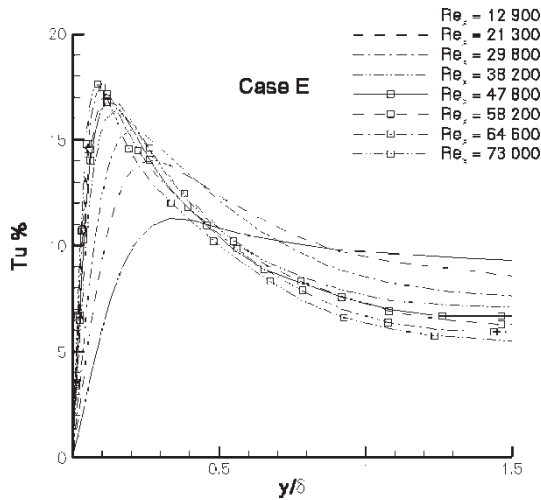


FIGURE 21 Spatial evolution of the turbulent level for case E.

The increase of u_{rms} , and hence of Tu , seems to come about partly from a transfer from v_{rms} inside the boundary layer. A reorganization of the turbulent structures in this region must be the origin of this phenomenon.

Examination of the turbulence level profile shows that peak Tu levels inside the boundary layer are about three times the outside turbulence level for all cases presented at $Re_x = 73,000$. Since initially the free-stream turbulent fields are substantially different, this is unlikely to be a coincidence.

The analysis of the turbulent energy production profiles reveals that Tu_{max} correspond to the location of maximum

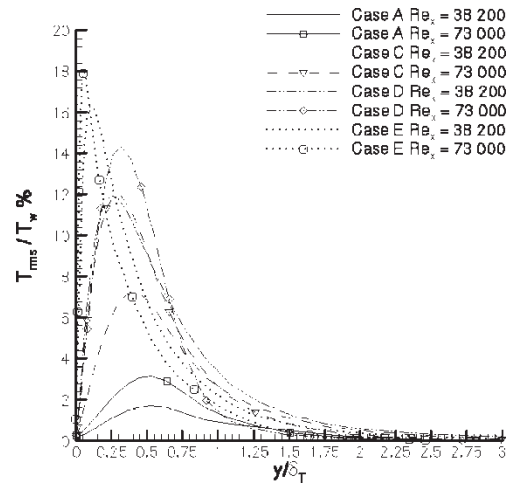


FIGURE 22 Thermal turbulent level for different cases.

turbulent energy production. Based on wall variables, this production is of the same order as the fully turbulent boundary layer. The preceding figures show how important the history of the development of the boundary layer under the free-stream turbulent field is in the analysis.

For the thermal boundary layer, we note in Fig. 22 that the thermal turbulent level is equal or slightly higher than Tu for the same case and Reynolds number. Outside the thermal boundary layer, temperature fluctuations are still present over a distance of at least δ_T while the free-stream thermal field is at constant temperature. This confirms the conclusion, drawn based on the turbulent

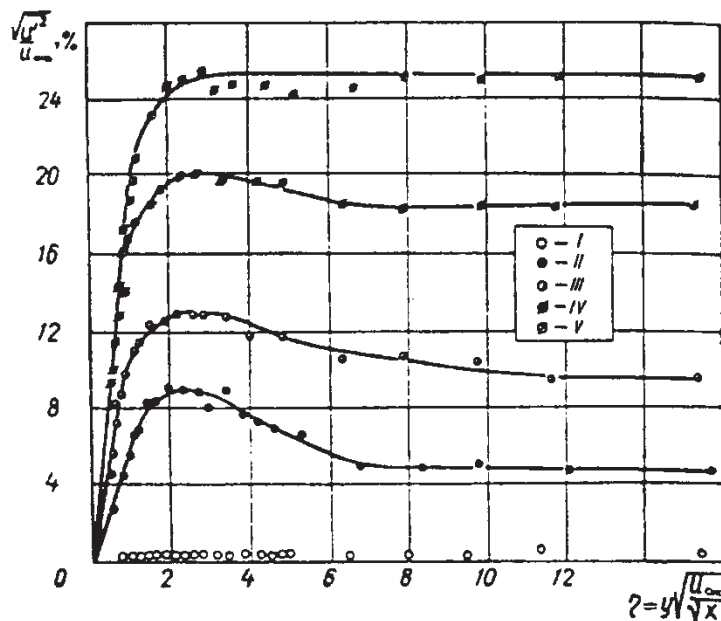


Fig. 3. Distribution of the pulsations in the laminar layer for $Re_\infty \cong 6.2 \cdot 10^3$: I— $\sqrt{(u'_\infty)^2}/U_\infty = 0.31\%$; II— 4.41% ; III— 9.69% ; IV— 18.4% ; V— 25.2% .

FIGURE 23 Extracted from Dyban *et al.* (1977) (legend from the article has been kept).

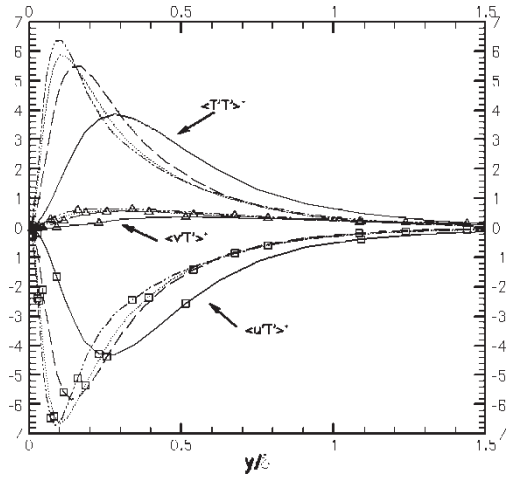


FIGURE 24 Spatial evolution of the velocity temperature correlation for case E. —: $Re_x = 16,800$; ---: $Re_x = 33,700$; ...: $Re_x = 55,000$; - · -: $Re_x = 71,900$.

Prandtl number, that the thermal boundary layer transfers more energy.

The analysis of the correlations $\langle T'T' \rangle$, $\langle u'T' \rangle$ and $\langle v'T' \rangle$ inside the boundary layer reveals that the temperature fluctuations are aligned with v' . However, although up to the peak of Tu_{\max} the amplitude of T_{rms} is directly correlated to u_{rms} , after that point the correlation weakens until, in the wake of the boundary layer $\langle u'T' \rangle < \langle T'T' \rangle < \langle v'T' \rangle$ (see Figs. 24 and 25).

We deduce that the thermal fluctuations are convected by the v velocity field and this explains why the temperature fluctuations do not vanish outside the boundary layer. From this analysis we can conclude that the v velocity field feeds the thermal boundary layer in turbulent energy through the wake. $\langle w'T' \rangle$ is negligible throughout the computational domain.

Figures 26–29 show the impact of the above phenomena on wall shear stress and heat transfer

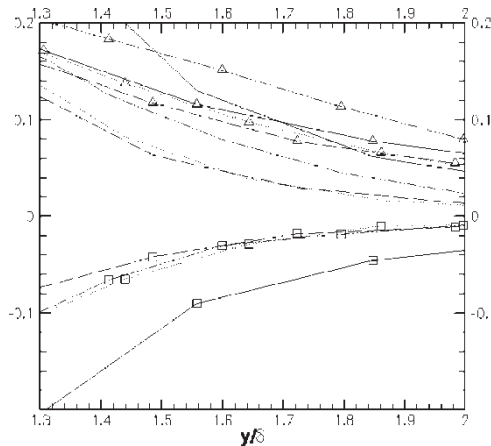


FIGURE 25 Spatial evolution of the velocity temperature correlation for case E. The same sign convention as in Fig. 24 is used —: $Re_x = 16,800$; ---: $Re_x = 33,700$; ...: $Re_x = 55,000$; - · -: $Re_x = 71,900$.

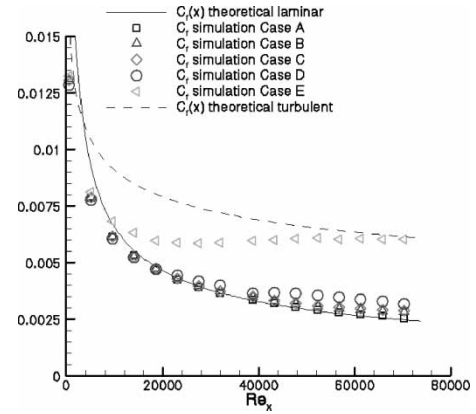


FIGURE 26 Influence of the free-stream turbulence on the friction coefficient.

coefficients, both of which are above the laminar values for $Re_x > 20,000$. This increase is linked to the amplitude of the free-stream turbulence level. For the case E, C_f and St reach the turbulent value at $Re_x \approx 70,000$ or $Re_\theta \approx 200$. For this case we note that wall coefficients do not change much for $Re_x > 20,000$, and as a first step to correlate wall transfer and free-stream turbulence a fit of the form $\sqrt{Re_x}$ is proposed for $C_f/C_{f,\text{lam}}$ and St/St_{lam} in Figs. 30 and 31.

Cases B and C in these figures exhibit the same increase of wall transfer and with no influence of the dissipative length scale. Furthermore, the temperature field is no more sensitive to free-stream turbulence than the velocity field since the same expressions fit the data. This appears to be in contradiction with the numerical and experimental observations. The answer to this contradiction lies in the rapid thickening of the boundary layers observed previously. Indeed, if instead of expressing the laminar value of C_f and St in terms of Re_x , we express them in

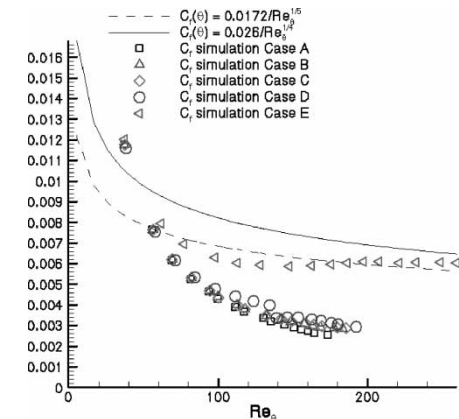


FIGURE 27 Influence of the free-stream turbulence on the friction coefficient based on the momentum thickness.

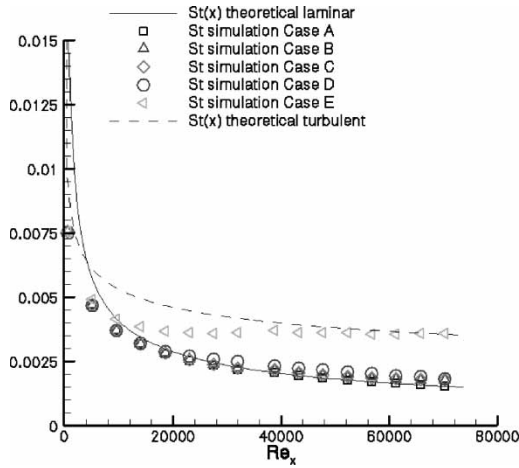


FIGURE 28 Influence of the free-stream turbulence on the Stanton number.

terms of $\delta(x)$, namely $C_f(x) = (3.32\nu)/(U_e\delta(x))$ and $St(x) = (1.66D)/(U_e\delta_T(x))$, we then obtain a completely different picture as shown in Figs. 32–35, and comparison between Figs. 33 and 35 does indeed reveal the higher sensitivity of the thermal field to free-stream turbulence.

The evolution of $C_f/C_{f, \text{lam}}$ and St/St_{lam} is also quite different as a linear variation is a good fit for the thermal field but a poor one for the dynamic field. The 500% increase for the Stanton number in Fig. 35 at $Re_x = 60,000$ does not represent the actual enhancement since the comparison is between two different boundary layers of the same thickness with and without free-stream turbulence. Locally, the heat transfer increase is of the order of 200% as shown in Fig. 31. This illustrates nonetheless the fastest spatial development of the thermal boundary layer. It is reasonable to expect that transition to turbulence for the thermal boundary layer might occur

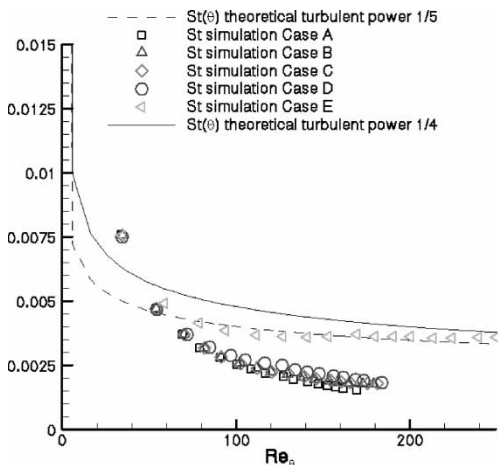


FIGURE 29 Influence of the free-stream turbulence on the Stanton number based on the momentum thickness.

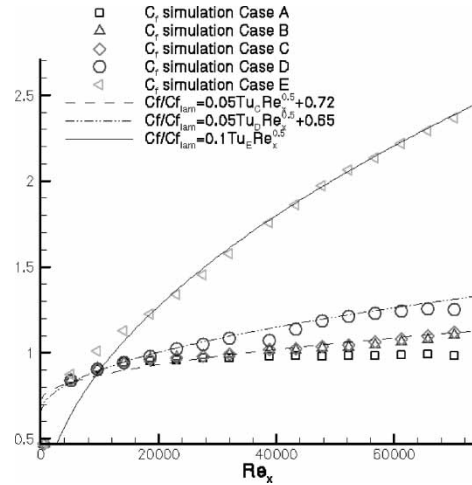


FIGURE 30 Friction coefficient ratio.

earlier, spatially speaking, since the thicker a boundary layer, the more unstable it is.

CONCLUSIONS

The influence of free-stream turbulence on the development of a boundary layer was investigated using LES. The experimental observations of Dyban *et al.* (1977), Dyban and Epick (1985) and Bradshaw *et al.* and others are well reproduced by the simulations, and detailed analysis of the LES data provides an explanation for many of these observations. The simulations also underscore the higher sensitivity of the thermal field to free-stream turbulence.

For all five cases presented here, bypass transition is found to occur in the early stage of the boundary layer development. Even if all the characteristics of a fully

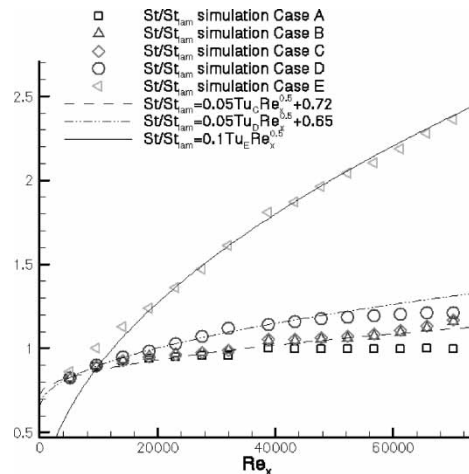


FIGURE 31 Stanton number ratio.

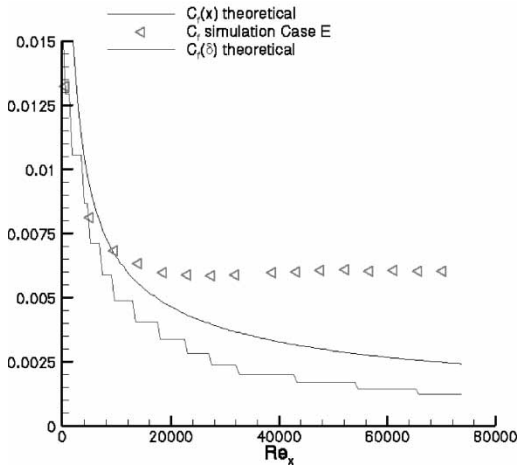


FIGURE 32 Influence of the free-stream turbulence on the friction coefficient based on the boundary layer thickness.

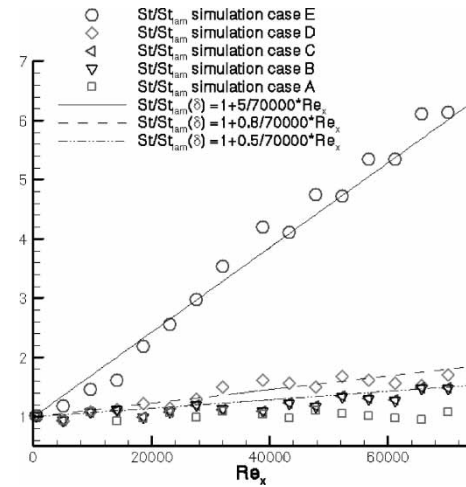


FIGURE 35 Stanton number ratio based on the thermal boundary layer thickness.

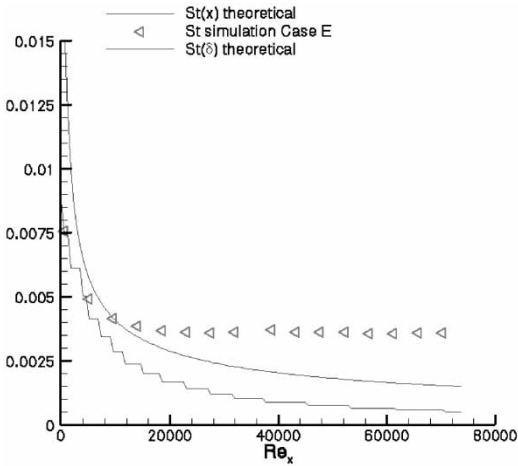


FIGURE 33 Influence of the free-stream turbulence on the Stanton number based on the thermal boundary layer thickness.

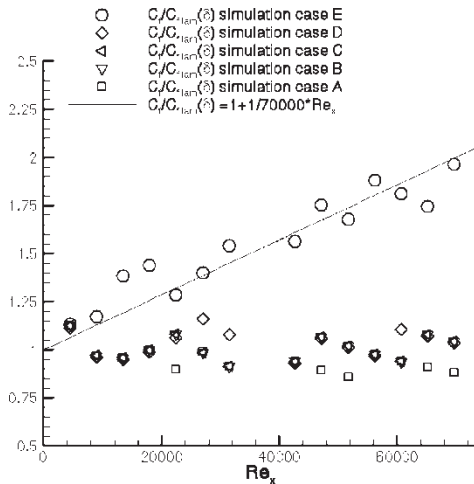


FIGURE 34 Friction coefficient ratio based on the boundary layer thickness.

turbulent boundary layer are not yet observable, the high level of turbulent intensity as well as the important flattening of the mean velocity and temperature profile suggest that, at least for case E ($Tu \approx 10\%$), the transition to turbulence takes place at a relatively low Reynolds number. Simulations in progress appear to confirm this point.

The next phase of this work is to simulate the interaction of the free-stream turbulence with the boundary layer region up to a Reynolds number where fully turbulent flow occurs to allow comparison with data from ongoing parallel investigation at INRA by Kondjuyan.

References

Baskaran, V., Abdellatif, O.E. and Bradshaw, P. (1989) "Effects of free-stream turbulence on turbulent boundary layers with convective heat transfer", In: University, S., ed, Seventh Symposium on Turbulent Shear Flows.

Blair, M.F. (1983a) "Influence of free-stream turbulence on turbulent boundary layer heat transfer and mean profile development. Part I—Experimental Data", *Journal of Heat Transfer* **105**, 33–40.

Blair, M.F. (1983b) "Influence of free-stream turbulence on turbulent boundary layer heat transfer and mean profile development. Part II—analysis of results", *Journal of Heat Transfer* **105**, 41–47.

Bradshaw, P. (1974). Effect of free-stream turbulence on turbulent shear layers, I.C., *Aero Report 74-10*, Imperial College of Science and Technology, Department Aeronautics, Prince Consort Road, London SW7 2BY.

Calmet, I. and Magnaudet, J. (1996) "Large eddy simulation of high Schmidt number mass transfer in a turbulent channel flow", *Phys. Fluids* **9**(2), 438–455.

Charnay, G., Comte-Bellot, S. and Mathieu, J. (1971) "Development of a turbulent boundary layer on a flat plate in an external turbulent flow", *ACARD Conf. Proc.*, 93.

Charnay, G., Comte-Bellot, S. and Mathieu, J. (1972) "Etat des Contraintes et des Fluctuations de Vitesse dans une Couche Limite Perturbée", *C.R. Acad. Sci. A* **274**, 1643.

Charnay, G., Comte-Bellot, S. and Mathieu, J. (1976) "Response of turbulent boundary layer to random fluctuations in the external stream", *Phys. Fluids* **19**(9), 1261–1271.

- Dyban, E.P. and Epick, E.Y. (1985). *Transferts de Chaleur et Hydrodynamique dans les Ecoulements Rendus Turbulents*. Monograph translated from Russian at I.N.R.A., available from A. Kondjoyan.
- Dyban, E.P., Epick, E.Y. and Surpun, T.T. (1977) "Characteristics of the laminar layer with increased turbulence of the outer stream", *Int. Chem. Eng.* **17**(3), 501–504.
- Fage, A. and Falkner, V.M. (1931) "On the relationship between heat transfer and surface friction for laminar flow", *Br. Aero. Res. Council R and M*, 1408.
- Hancock, P.E. and Bradshaw, P. (1983) "The effect of free-stream turbulence on turbulent boundary layers", *J. Fluids. Eng.* **105**, 284–289.
- Hancock, P.E. and Bradshaw, P. (1989) "Turbulence structure of a boundary layer beneath a turbulent free-stream", *J. Fluid. Mech.* **205**, 45–76.
- Kondjoyan, A., Péneau, F. and Boisson, H.C. (2002) "Effect of high free-stream turbulence on heat transfer between plates and air flows: a review of existing experimental results", *Int. J. Therm. Sci.* **41**, 1–16.
- Maciejewski, P.K. and Moffat, R.J. (1992) "Heat transfer with very high free-stream turbulence: part II analysis of the results", *ASME J. Heat Transfer* **114**, 834–839.
- Meier, H.U. and Kreplin, H.P. (1980) "Influence of free-stream turbulence on boundary-layer development", *AIAA* **18**(1), 11–15.
- Pédissius, A.A., Kazimekas, P.V. and Slanciauskas, A.A. (1979) "Heat transfer from a plate to a high-turbulence airflow", *Heat Transfer Soviet Res.* **11**(5), 125–134.
- Péneau, F., Legendre, D., Magnaudet, J. and Boisson, H.C. (1999) "Large eddy simulation of a spatially growing boundary layer using a dynamic mixed subgrid-scale model", Symposium ERCOFTAC on Direct and Large Eddy Simulation, (Cambridge).
- Péneau, F., Boisson, H.C. and Djilali, N. (2000) "Large eddy simulation of the influence of high free-stream turbulence on a spatially evolving boundary layer", *Int. J. Heat and Fluid Flow* **21**, 640–647.
- Simonich, J.C. and Bradshaw, P. (1978) "Effect of free-stream turbulence on heat transfer through a turbulent boundary layer", *Trans. ASME J. of Heat Transfer* **100**, 671–677.
- Smagorinsky, J. (1963) "General circulation experiments with the primitive equations", *Mon. Weather Rev.* **93**, 99.
- Young, C.D., Han, Y., Huang, Y. and Rivir, R.B. (1992) "Influence of jet grid turbulence on flat plate turbulent boundary layer and heat transfer", *J. Heat Transfer* **114**, 64–72.
- Zang, Y., Street, R.L. and Koseff, J.R. (1993) "A dynamic mixed subgrid-scale model and its application to turbulent recirculating flows", *Phys. Fluids* **A5**(12), 3186–3196.